ASTM INTERNATIONAL

Geotechnical
Testing Journal

G. Viggiani,[1] E. Andò,[2] D. Takano,[3] and J. C. Santamarina[4]

DOI: 10.1520/GTJ20140060

Laboratory X-ray Tomography: A Valuable Experimental Tool for Revealing Processes in Soils

VOL. 38 / NO. 1 / JANUARY 2015

Geotechnical Testing Journal

doi:10.1520/GTJ20140060 / Vol. 38 / No. 1 / January 2015 / available online at www.astm.org

G. Viggiani,[1] E. Andò,[2] D. Takano,[3] and J. C. Santamarina[4]

Laboratory X-ray Tomography: A Valuable Experimental Tool for Revealing Processes in Soils

Reference

Viggiani, G., Andò, E., Takano, D., and Santamarina, J. C., "Laboratory X-ray Tomography: A Valuable Experimental Tool for Revealing Processes in Soils," *Geotechnical Testing Journal*, Vol. 38, No. 1, 2015, pp. 61–71, doi:10.1520/GTJ20140060. ISSN 0149-6115

Manuscript received March 22, 2014; accepted for publication September 15, 2014; published online October 14, 2014.

[1] Univ. Grenoble Alpes, 3SR, F-38000 Grenoble, France.

[2] CNRS, 3SR, F-38000 Grenoble, France.

[3] Geotechnical Engineering Division, Port and Airport Research Institute, Yokosuka City, Kanagawa, 239-0826, Japan.

[4] School of Civil and Environmental Engineering, Georgia Institute of Technology, Atlanta, Georgia, 30332, USA.

ABSTRACT

The use of high-resolution tomographic techniques has allowed for unprecedented observations and a renewed understanding of geomaterials and processes. A laboratory x-ray scanner is used to explore the potential of the technology in the context of complex geotechnical systems. Tests benefit from the fast and non-destructive nature of x-ray measurements and the micrometer-scale resolution that is attainable. Several first-time observations are reported here. In this paper we demonstrate the following: subsurface volume loss in sandy soils can cause the formation of sharply defined low-density pipes; cryogenic suction consolidates sediments next to ice lenses during ground freezing; root growth involves transverse expansion, and the stress relaxation at the tip facilitates further longitudinal invasion; blade insertion causes successive shear localizations; and the incipient formation of desiccation cracks is not necessarily along a planar front—in fact, the fracture plane may split as it encounters heterogeneities at the tip. Finally, it is shown that x-rays can be used to monitor chemical processes that cause coupled mechanical effects, such as osmotic consolidation induced by ionic diffusion and mineral dissolution. Although brief events may not be tomographically imaged, single x-ray radiographs can be analyzed and compared to gain extensive process information.

Keywords

x-ray micro-tomography, heterogeneity, spatial variability, localization, frozen ground, roots, desiccation cracks

Introduction

Most laboratory soil characterization is based on observations of specimen boundaries, where forces, deformations, energy potential, and flow are either imposed or measured. Measurements are then interpreted to determine material behavior using constitutive equations in terms of stress, strain, flow rate, and gradients. This approach assumes homogeneity within the specimen and is therefore inadequate for the study of non-homogeneous processes; the study of such processes requires field measurements. Full-field methods have been extensively used in experimental geomechanics; examples include magnetic resonance imaging (e.g., Sheppard et al. 2003), positron emission tomography (e.g., Kulenkampff et al. 2008), x-ray tomography (e.g., Andò et al. 2012), electrical resistivity tomography (e.g., Comina et al. 2008), and neutron tomography (e.g., Hall 2013). Viggiani and Hall (2012) published a recent review of full-field techniques in geomechanics.

The use of x-ray imaging in experimental geomechanics dates back to the 1960s (e.g., Roscoe 1970). X-rays were used to obtain two-dimensional (2D) radiographs on photographic plates. Radiographs represent maps of attenuation accumulated along the ray path through the soil mass. These early studies lacked quantitative measurements of the observed attenuation/density changes and were limited to 2D observations. Both limitations are overcome by x-ray computed tomography (CT), in which radiographs obtained at many different angular positions are used to reconstruct a three-dimensional (3D) field of x-ray attenuation (closely related to mass density) (Baruchel 2000; Stock 2008). First developed for medical imaging, x-ray CT is now widely used in material sciences, geosciences, and geomechanics (*e.g.*, Otani and Obara 2004; Desrues et al. 2006; Alshibli and Reed 2010). The 3D images or fields coming from x-ray CT are composed of voxels (3D pixels) whose values can be interpreted as a mean local density when the voxels are significantly larger than the grain size; alternatively, one can delineate individual grains when the voxels are significantly smaller than the grains. The 3D tomographic images provide unprecedented insight into the nature and complexity of bio-, hydro-, thermo-, chemo-, and mechanical processes taking place within a soil mass. Consequently, many laboratories around the world have been deploying this technology, either adapted from medical systems or specifically designed to address materials research, to learn about soils and soil processes. It is worth noting that besides laboratory scanners, there is also the possibility of using synchrotron facilities for x-ray imaging. These facilities provide a much more powerful source of x-rays allowing both fast scanning and high spatial resolution, as well as more advanced imaging techniques such as phase contrast tomography. Although synchrotron facilities are used in geomechanics applications (e.g., Viggiani et al. 2004; Hall et al. 2010; Fusseis et al. 2014), they are limited in number (about 40 worldwide), and access is also limited.

This paper shows the power of full-field x-ray tomography (using a lab scanner) to shed light on a number of non-homogeneous processes in soils. The experiments were conducted in the x-ray scanner in Laboratoire 3SR (Grenoble, France). Emphasis is placed on observations that are only possible using this technology. This manuscript presents a brief description of the device followed by a discussion of several exploratory studies.

X-ray Tomography: Description of the Imaging Device Used in this Study

The setup for x-ray tomography used in this study is shown in **Fig. 1**. It includes a Hamamatsu L8121-03 micro-focus x-ray source emitting a cone beam and a 1920 by 1536 pixel 14-bit x-ray flat panel detector (Varian PaxScan 2520V, measuring 195.07 by 243.84 mm, meaning that each pixel measures 0.127 by 0.127 mm on the detector). The sample to be scanned is placed between the source and the detector on a translation and rotation stage. Rotation is necessary for the specimen to be imaged at different angular positions. Translation (in the axis of the beam) allows control of the distance between the sample and the source, which in turn controls the size of the image that

FIG. 1 X-ray tomographic system for geotechnical studies. (*a*) The device at Grenoble has a maximum resolution of 5 μm. (*b*) The specimen holder is designed for high-precision re-mounting so that long-term processes can be re-imaged at predefined time intervals.

(a)

(b)

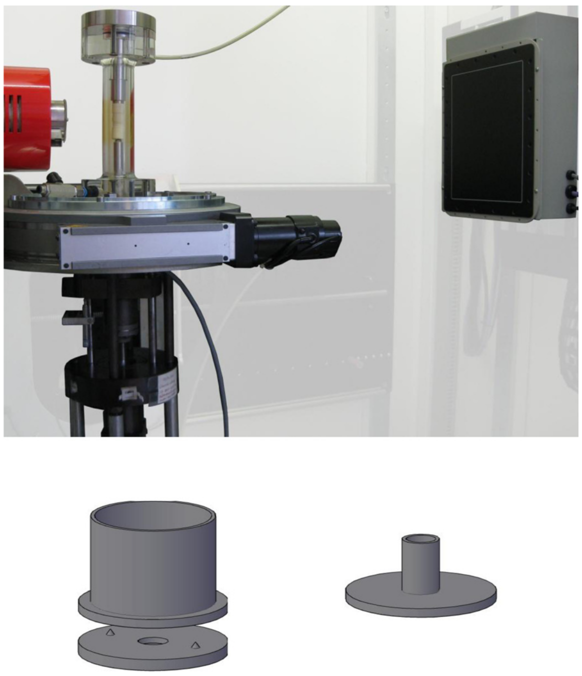

is projected onto the detector (zoom). The range of x-ray energy that can be generated by the source is 40 to 150 keV, allowing a range of different sample sizes and densities to be imaged. The spatial resolution (expressed in terms of voxel size) depends on the "zoom" level (i.e., the distance between the sample and the source); it cannot be smaller than the smallest spot size (5 μm in low-power mode) and is limited upward by the physical size of the detector. Scanning time depends on the number of angular positions imaged, the number of images averaged at each angular position (in order to increase the signal-to-noise ratio), and the time needed for each image (equivalent to exposure time in photography). The "exposure time" is chosen depending on the x-ray attenuation of the sample and the power used. Although very precise measurements can be made using long scanning times, these scans are vulnerable to differential displacements in the imaging system that may occur over several hours as a result of temperature fluctuations.

There are trade-offs between specimen size and resolution, as well as between scan time and process time. The scans presented in this paper were not performed at the highest possible zoom level because of the size of the specimens and the desire to perform fast scans at high power for short-duration events. Each scan involved radiographs acquired at 1200 equally spaced angular positions and the averaging of four to ten images per angular position to enhance the signal-to-noise ratio, giving a scan time between 30 and 60 min.

Exploratory Studies—Unprecedented Observations

The processes selected for these exploratory studies cover a wide range of problems in soil mechanics, ranging from the classical trapdoor experiment to ice lens formation and root growth in soils. Each process, along with salient results, is described in the following sections.

SOIL DEFORMATION DUE TO VOLUME REMOVAL

Ground loss at the head of tunnels and in mining operations is a classical geotechnical problem with important implications for infrastructure development in urban settings (e.g., Gonzàles and Sagaseta 2001). Although ground loss depends on a number of factors, including the tunneling method (*e.g.*, Ng et al. 2004), at the laboratory scale, the trapdoor experiment (see the classical work by Terzaghi [1936], recently revisited using x-ray tomography by Takano et al. [2004]) is often used as a simplified yet useful model for providing some understanding of ground loss in actual engineering situations.

In this study we aimed to investigate the deformation field in a cylindrical soil mass when soil is removed from the bottom of the cylinder. The specimen was prepared in a Plexiglas cylinder (diameter, 94.6 mm; height, 98 mm). It consisted of ten layers of a uniform siliceous fine sand (dry density $\gamma = 17.05\ \mathrm{kN/m^3}$, $e = 0.554$, $D_{50} = 0.2$ mm) with thin layers of crushed mica (deposited by raining) that acted as tracers in the scans by means of their different densities. The cell had a 2.5-mm port at the bottom to allow for sand extraction. Two scans were performed at a spatial resolution of 70 μm/voxel: the first captured the as-built specimen, and the second showed the specimen after 4.1 g of sand had been extracted from the bottom hole.

A central slice of the second 3D tomogram shown in **Fig. 2** clearly reveals a lighter carrot-shaped pipe of lower density than the surrounding material ($\gamma = 14.5\ \mathrm{kN/m^3}$, $e = 0.828$). The pipe extends along the entire specimen height, piercing the surface,

FIG. 2

Density changes: formation of a low-density pipe structure upon the extraction of a small volume of sand from a central port at the bottom of the specimen. The horizontal lines on the x-ray image are thin monolayers of mica plates used as tracers. The position of mica plates inside the pipe documents shear-limited granular flow. The horizontal density profile (shown directly on the x-ray image and expressed in terms of the void ratio) shows a sharp contrast between the denser host sand (near e_{min}) and the loosened sand in the pipe (near e_{max}).

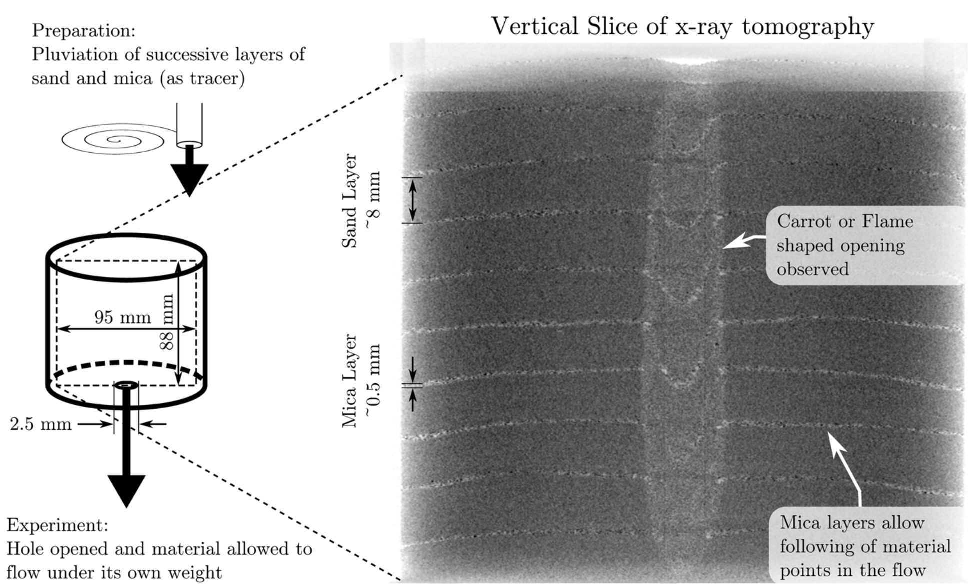

and a small depression is noticed at the top free surface. The pipe volume measured in the 3D image is much larger than the extracted volume (11.2 cm^3 versus 2.3 cm^3). Granular flow remained highly focused throughout the specimen height; the maximum width of the pipe was measured as 13.7 mm, compared to the 2.5-mm opening in the bottom of the cylinder.

The void ratio profile superposed on the x-ray image in **Fig. 2** shows a sharp transition in density between pipe and surrounding material. The sediment density in the pipe fluctuates along the depth; however, there is no sufficient evidence to conclude that these are density waves within the pipe (as observed by Peng and Herrmann [1994]). The position of the mica platelets shows that grain displacement within the pipe is quasi-parabolic with edge slippage or shear localization at the pipe–medium interface.

ICE FORMATION IN SOILS

Ice formation in soils plays a fundamental role in frost-induced heaving, which is of obvious concern for any geotechnical structure in regions susceptible to freezing temperatures (Dysli 1991; Sheng et al. 1995). Although complex, the mechanics of ice formation in soils can be revealed by x-rays, as suggested, for example, by Torrance et al. (2008).

The water–ice interfacial tension is $T_s \approx 32$ mN/m (compared to 72 mN/m for water–air). Therefore, a Laplacian pressure Δu develops in the ice that is directly proportional to the interfacial tension and inversely proportional to pore size d_{pore}: $\Delta u = 4T_s/d_{pore}$. Then, similar to desiccation cracks, we can anticipate the development of segregated ice lenses when capillary forces exceed the skeletal forces as a result of effective stress ($N = d^2\sigma'$), that is, in fine-grained materials with small d_{pore} and subjected to low effective stress (Dai et al. 2012).

Several tests were performed to explore the topology of ice formation during soil freezing. In the first set of tests, three water-saturated soil specimens (fine Fontainebleau sand with $D_{50} = 156\ \mu$m, kaolinite, and bentonite) were prepared in a Plexiglas cylinder (diameter, 80 mm; height, 110 mm) and placed in a freezer for 24 h ($T = -18°$C). Kaolinite and bentonite specimens were prepared at initial water contents equal to their liquid limits. After freezing, each specimen was scanned at a spatial resolution of 50 μm/voxel. **Figure 3** shows slices of the corresponding 3D images. The sand specimen shows no evidence of ice segregation, as anticipated. Lenses grew inward from the specimen boundary in the kaolinite specimen. The bentonite specimen was massively crisscrossed by ice lenses. Density profiles across the lenses show a relatively constant density in the soil mass next to lenses [*e.g.*, **Fig. 3(*d*)**]. The absence of a density gradient in the soil close to lenses indicates that cryogenic suction-driven consolidation has been completed. Stable temperature conditions were reached in the three specimens (the time scale of thermal diffusion is less than one hour $\sim L^2/D_t$); therefore, the observed morphology reflects lens saturation at steady-state conditions. Ice lens formation is a 3D phenomenon; **Fig. 3(*e*)** shows several horizontal slices, taken at different heights, for the kaolinite specimen. Several major ice lenses can be followed from slice to slice; this shows that these lenses grow quasi-vertically. This is consistent with the general observation that opening mode discontinuities form normal to the minor principal stress (horizontal in this case).

A second experiment was conducted on water-saturated kaolinite paste mixed at $w \approx 2$LL (twice the Atterberg liquid limit) and left in the freezer for 24 h (Plexiglas cylinder diameter, 94.6 mm; height, 98 mm). As freezing progressed, paste extruded through the frozen upper crust and formed a $\sim$2-cm^3 protuberance on the surface [see **Fig. 4(*a*)**]. The morphological complexity hidden in the specimen cannot be conceived by observing ice lenses at the boundary through the transparent container. The 3D tomography (at 70 μm/voxel) revealed that lenses closest to the periphery appeared to have grown inward, much like with the previous kaolinite specimen [see **Figs. 3(*c*)**, **4(*b*)**, and **4(*c*)**]. The high lens density on the periphery reflects the initially high water content. The lens pattern gradually transformed into a layered, onion-like structure with no ice lenses in the core. This pattern reflects the interplay among ice lens formation, stress changes, and the evolving sediment porosity with cryo-suction. The stress relief associated with paste extrusion at the surface changes the orientation of the lenses around the specimen core. The radial density profile in **Fig. 4(*d*)** shows homogeneous density in the soil at the core of the specimen and sections of soil between lenses having the same density value (i.e., steady-state condition). Lens saturation implies that not all the water is available for freezing and ice lens formation at a given temperature, as anticipated by the Laplace-Thompson equation (Santamarina and Jang 2010).

The previous tomograms were measured at steady state. A third experiment was specifically designed to check whether a consolidation front caused by cryogenic suction could be detected with x-ray tomography. A 125-mm-high, water-saturated kaolinite specimen was prepared at $w = 2$LL (container diameter, 94.6 mm) and then subjected to a low-temperature upper boundary by adding dry ice (at $-78°$C). The early advancement of the freezing front was monitored with x-ray radiographs (first 2 h). A 3D image was then acquired at 70-μm resolution (a slice of which is shown in **Fig. 5**). The density profile in **Fig. 5** clearly shows a 25-mm-thick layer of frozen kaolinite followed by a 30-mm-thick zone where the soil is consolidated in response to the gradient created by cryogenic suction. The lower region remained undisturbed at the initial conditions.

This collection of experimental observations and measurements is potentially valuable data to inform and validate existing models, such as those by Konrad and coworkers (*e.g.*, Konrad and Duquennoi 1993).

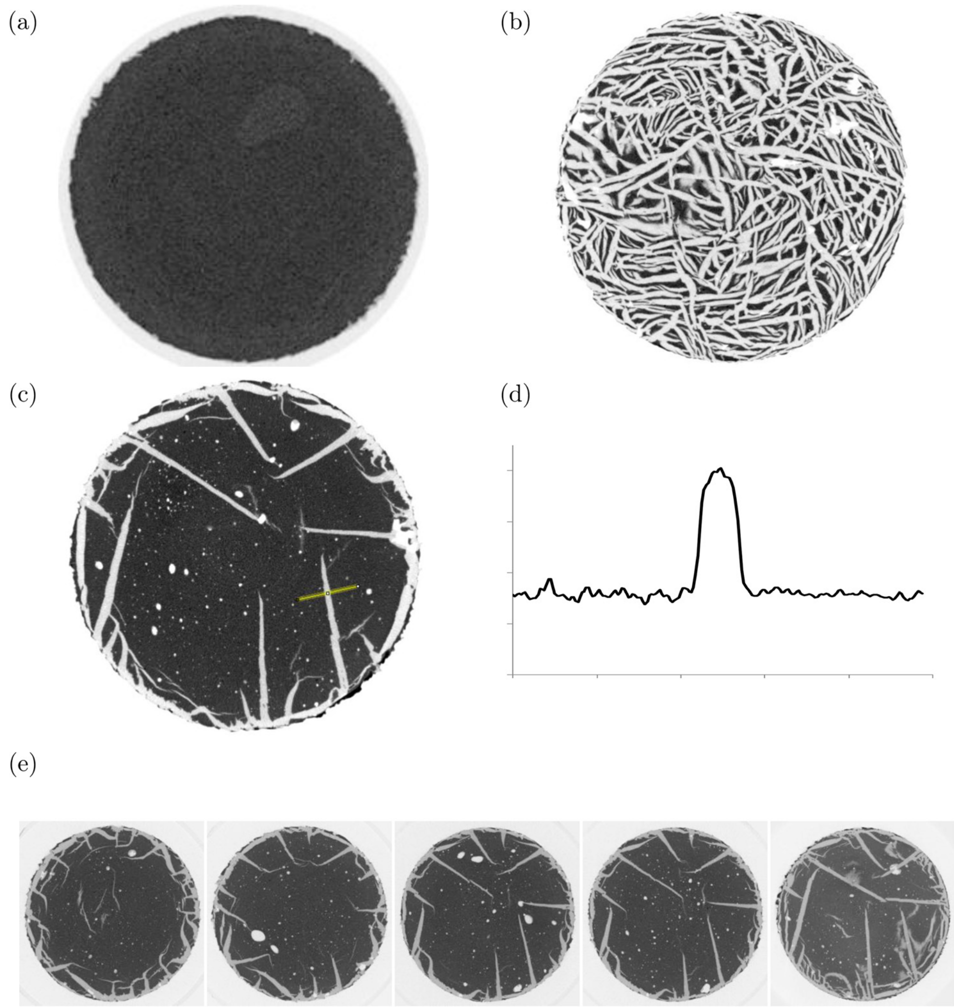

FIG. 3

Frozen ground. (*a*) Fine sand (no lenses). (*b*) Bentonite paste mixed at a water content near the liquid limit $w \approx$ LL. (*c*) Kaolinite mixed at $w \approx$ LL. (*d*) Density profiles shown across an ice lens in the kaolinite specimen. (*e*) Slices of different elevations from the upper and lower boundaries of the kaolinite specimen. Note: light color corresponds to ice, and dark color to sediment.

BEAN SEED GROWTH IN SAND

Opening-mode discontinuities in granular soils can be driven by fluid flow (hydraulic fracture), capillarity (desiccation cracks or gas-driven fractures), or ice pressure (ice lenses; see "Ice Formation in Soils," or refer to the work of Shin and Santamarina [2011b]). From the sediment perspective, root growth is an opening-mode discontinuity, but in this case it is driven by the pressure that the root exerts against soil grains (early studies date from the late 19th century [Pfeffer 1893; Savioli et al. 2014]).

The pressure inside cells is of an osmotic nature because of the higher ionic concentration inside cells than in the surrounding fluid. This "turgor" pressure causes cell expansion; the root swells normal to its axis behind the tip, and the radial stress decreases ahead of the tip. This stress field facilitates cell splitting at the tip and cell expansion ahead of the tip. It follows from this discussion that root growth both is affected by and alters the state of stress in the soil mass. The ensuing root architecture was initially studied by terminating tests; the first tomographic studies used low-resolution medical devices (1.5-mm voxels [Hainsworth and Aylmore 1983]), and higher resolution was obtained with industrial devices and specially designed scanners (150 μm [Gregory et al. 2003]).

Red beans were placed in moist paper to start germination and then planted 45 h later in partially saturated 40–60 Ottawa sand (grain diameter ranging from 250 to 420 μm, with a degree of saturation close to 50 %). Tomographic images were acquired at 30-μm resolution every 24 h. Two similar germination specimens were monitored; both plants survived the study with no evident damage caused by the x-ray scans.

Images in **Fig. 6** show the seed-root system at different stages of growth. These images were obtained by thresholding out the seed and hiding the sand for the purposes of presentation. Because of the inhomogeneous nature of the density distribution in both sand and seed, some "erode-dilate" cycles were used to fill some holes on the boundary between both "phases." This procedure, coupled with the fact that there is a partial

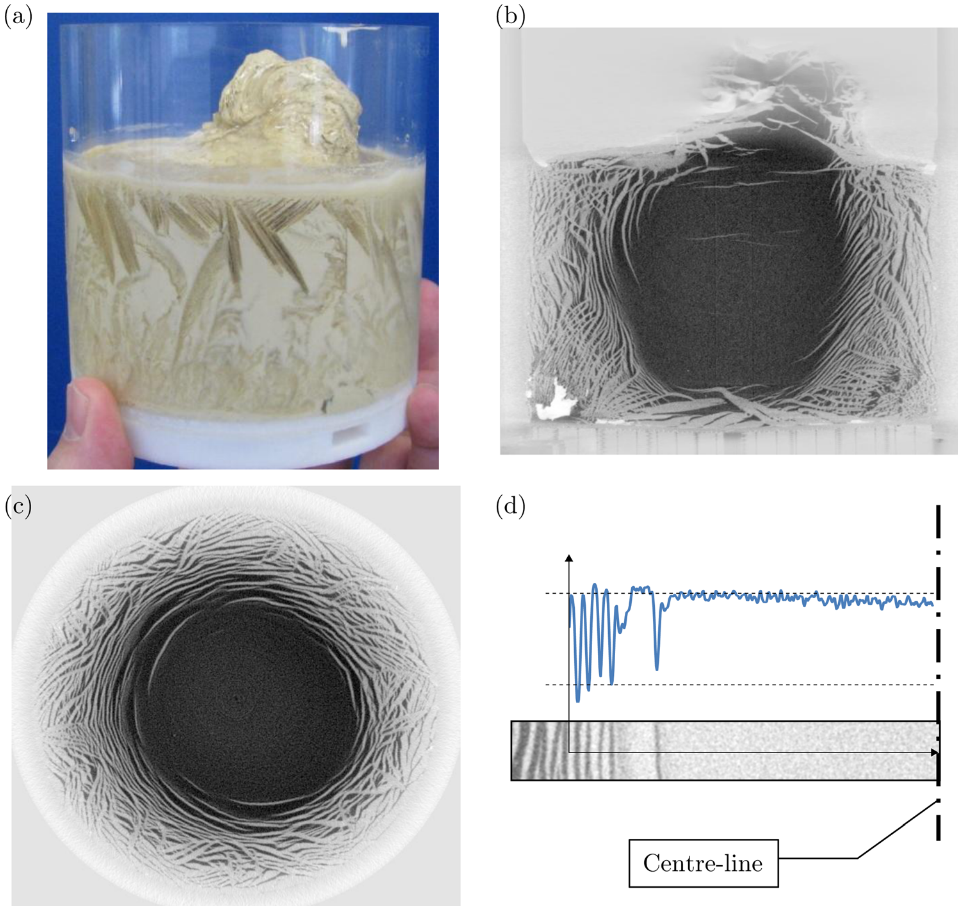

FIG. 4
Frozen kaolin paste mixed at a water content $w \approx 2LL$. (*a*) External view. (*b*) Vertical and (*c*) horizontal cross-sections. The initial set of ice lenses formed around the periphery and grew radially into the specimen; the second, internal set formed concentrically, probably after the clay paste broke through the frozen upper crust. (*d*) Radial density profile: the clay had a similar density between ice lenses and toward the center of the specimen; this observation is consistent with ice lens saturation.

volume effect between these two phases, led to a small degree of artificial surface roughness, as can be seen in **Fig. 6**.

Figure 7 shows the seed five days after the beginning of the experiment (i.e., from the first wetting). New growth at the tip of the root in the last 24 h has considerable surface roughness relative to the more mature part of the root above [**Figs. 7(*b*)** and **7(*c*)**]. The tip surface roughness indicates that root growth in this coarse sand was at the verge of pore invasion [**Fig. 7(*c*)**]. In other words, cell splitting and growth at the tip are favored in the unconstrained pore space, rather than where grain surfaces press against the root.

Complementary Studies

Several complementary studies were conducted as part of this investigation to gain additional information about the power and limitations of x-ray tomography. Salient observations follow.

DENSITY CONTRAST: WEDGE INSERTION

The tomographic image in **Fig. 8(*a*)** was obtained after the insertion of a plastic wedge in a silt specimen. The image shows that successive shear bands developed during insertion. The causal link between x-ray attenuation and mass density makes x-ray imaging an exceptional tool for the study of shear localization, from the early 2D images (Roscoe 1970) to the remarkable success of 3D tomograms (Desrues et al. 1996). For comparison, note that no evidence of shear bands was observed in any of the cases of opening-mode discontinuities imaged in this study, that is, desiccation cracks, ice lenses, and roots.

CONTRAST—DESICCATION CRACKS

X-ray tomography is particularly well suited for the study of desiccation cracks because of the high contrast between air and soil absorption (in other applications where contrast may be lacking, the experimental method may be altered to explicitly include high- and low-absorption components, such as iron or barium and plastic or foam). A cross-section of a desiccation crack in bentonite is shown in **Fig. 8(*e*)** (initial water content $w \approx LL$). The density profile across the crack shows no evidence of changes in density in the area around this opening-mode discontinuity [**Fig. 8(*f*)**]; this suggests that the water–air interfacial membrane did not penetrate the soil behind the crack face and the soil mass remained saturated (Shin and Santamarina

FIG. 5

Cryogenic suction. The clay paste mixed at a water content $w \approx 2LL$ was subjected to a thermal gradient to create a stable frozen front (dry ice at the top and 18°C at the bottom). The gray scale and the superimposed density profile confirm the presence of a higher density zone beneath the frozen layer. This ~20-mm-thick zone shows increased density because it has been consolidated by cryogenic suction.

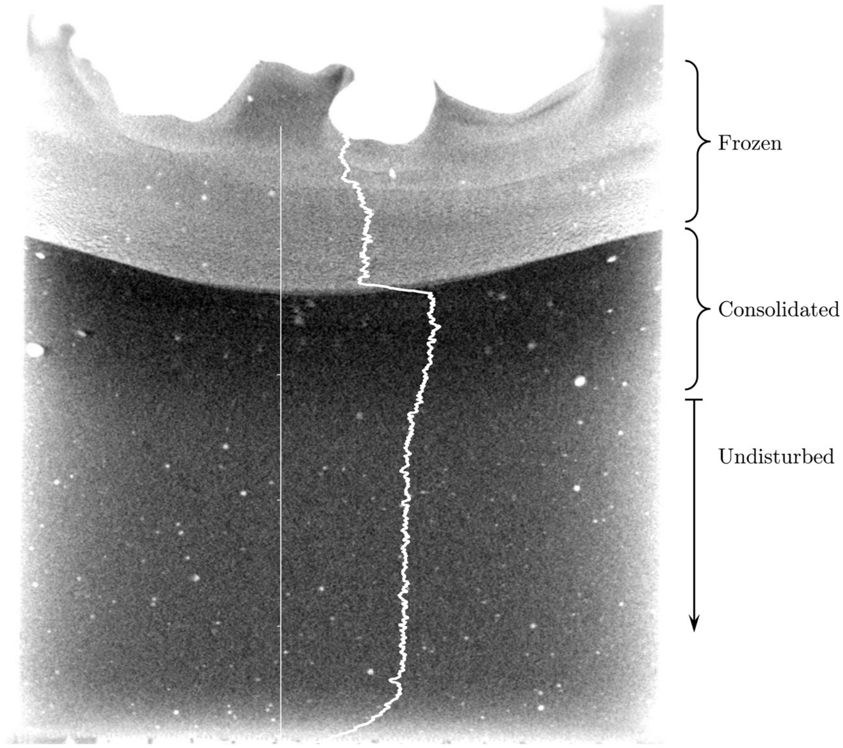

FIG. 6

Bean-root system: evolution during germination (*a*) 4 days, (*b*) 5 days, (*c*) 6 days, and (*d*) 7 days after wetting. The transverse root system that starts developing from the main root after the fifth day will provide reaction capacity to pull the bean out of the ground and stability to the growing plant.

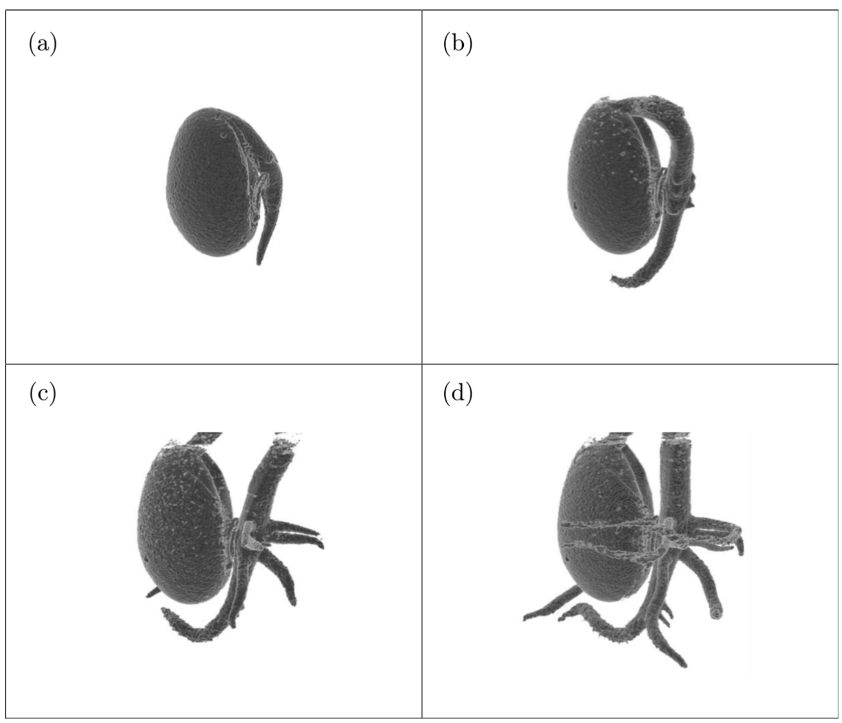

FIG. 7 Bean-root system 5 days after wetting. (*a*) Developing root and selected cross-section planes. (*b*) The upper part of the root is older and thicker, and it has already gained a quasi-circular cross-section. (*c*) The younger tip of the root has grown in the last 24 h and shows early cell growth into pores.

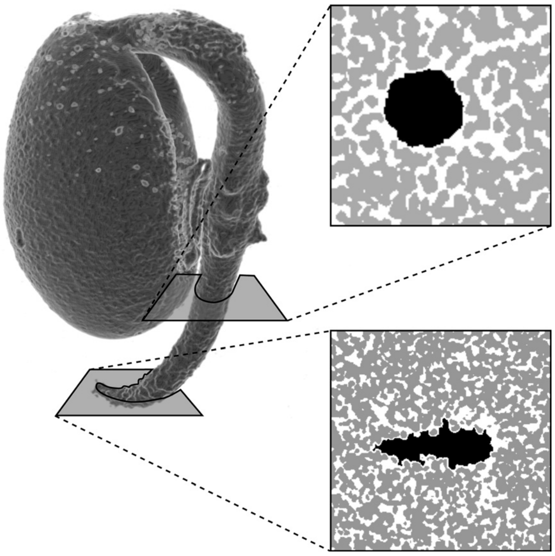

2011a). Fracture fronts are not necessarily continuous, and several splits can be observed.

DETECTING CAUSE OR EFFECT? DIFFUSION AND OSMOTIC CONSOLIDATION

The resolution of x-ray tomography might not be sufficient to monitor a given process on its own; however, the technique can be used to detect a coupled effect. This is the case for a diffusing high-ionic-concentration front: although x-ray absorption cannot visualize the propagating front, the ensuing osmotic consolidation might give a detectable signature. This concept was explored using a Plexiglas cell ($d = 80$ mm, $h = 110$ mm) filled with a kaolinite–bentonite paste (PL = 30, LL = 160; mixed at $w \approx$ LL, with PL and LL being the plastic and the liquid limit, respectively). A central cylindrical orifice ($d_{cyl} = 10$ mm, $h = 25$ mm) was filled with a high-salt NaCl brine ($c = 6$ M), and the cell was enclosed to prevent moisture loss. The x-ray tomogram obtained 4.6 days after preparation revealed a denser zone surrounding the orifice (i.e., osmotic consolidation) [**Figs. 8(*c*)** and **8(*d*)**].

FIG. 8 Other exploratory studies. (*a*) Wedge insertion and shear bands. (*b*) Short-time water invasion: differential radiographs. (*c*), (*d*) Ionic diffusion and ensuing osmotic consolidation with density profile. (*e*), (*f*) Desiccation crack with transverse density profile.

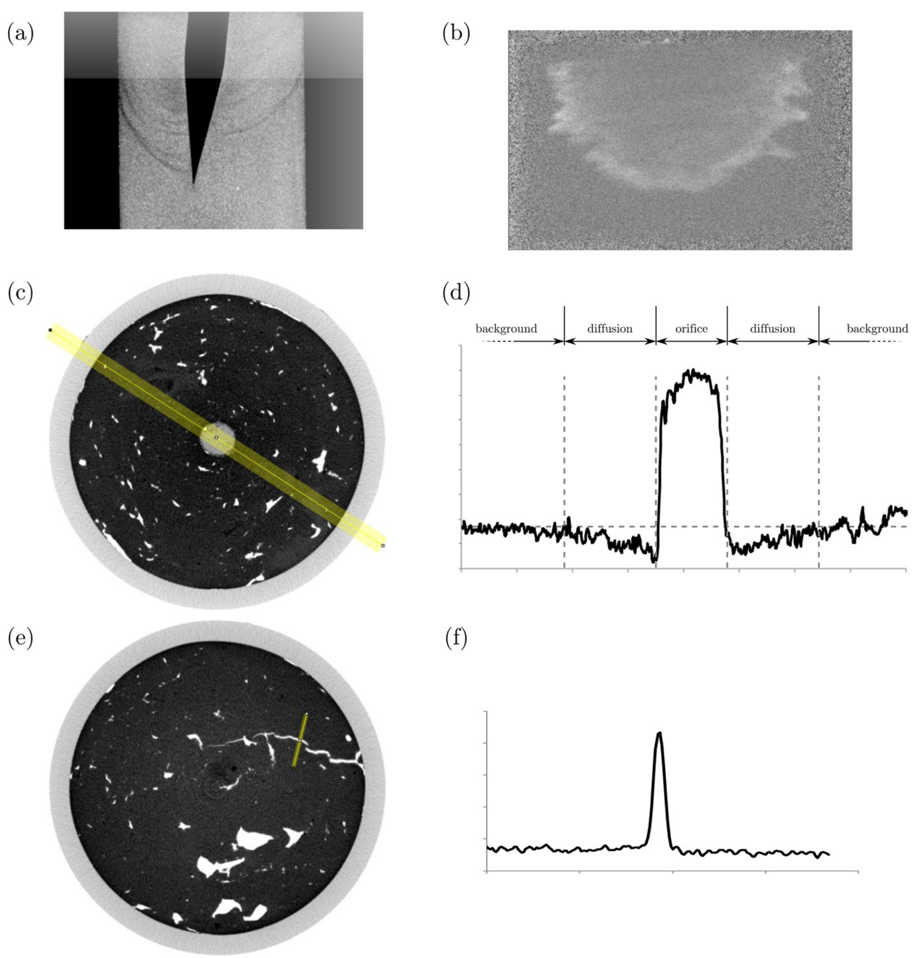

PROCESS TIME AND DEBORAH'S NUMBER: WETTING FRONTS

A tomographic image presumes quasi-static time-invariant conditions during data collection; that is, the process time is much longer than the observation time, or there is a high Deborah's number (meaning that the material behaves more like an elastic solid than a fluid) (Reiner 1964). Currently, data collection for a high-resolution tomogram in a lab scanner can take 30 min or more. Therefore, the process time must be on the order of days, as in the case of roots. Although full tomographic imaging is not possible in short time processes, successive x-ray images (duration $\delta_t < 0.1$ s) can provide valuable information. **Figure 8(*b*)** shows the image difference between two successive radiographs gathered 6 s apart of a dry sand being invaded by water. Although this is a 2D projection of the 3D phenomenon, the image permits the detection of the topology of gravity-driven invasion along regions with greater porosity. Recent x-ray tomography developments in synchrotron facilities have hugely reduced tomogram acquisition times to a few seconds, allowing further investigation of such phenomena in 3D; see, for example, the report by Berg et al. (2013).

Conclusions

X-ray tomographic imaging provides unprecedented capabilities for the study of geomaterials and processes. The technology is simple, accessible, and readily adoptable for geotechnical applications. Therefore, x-ray tomographic imaging allows old questions to be revisited with relatively low experimental effort, yet with the promise of gaining great insight and the potential for surprising observations of unexpected structures.

X-ray tomography is non-destructive, even for biological components, and supports characterization before, during, and after processes. In other words, this technology allows process monitoring in 3D + time. The trade-offs between range and resolution and between process and measurement time scales are linked through an inherent experimental requirement: high resolution demands a longer scanning time.

The application of x-ray tomography to the study of processes in sediments has stimulated the development of innovative measurement and data processing protocols including 3D digital image correlation (discrete [i.e., grain-based] [Andò et al. 2012) and continuum [i.e., pattern-based] [Smith et al. 2002]), assessment of grain-level forces (Hall et al. 2011; Alshibli et al. 2013), combined measurements (e.g., x-ray with acoustic tomography), and complementary tomography–finite element method analyses (Besnard et al. 2006). These developments allow us to enhance the interpretation of conventional tests (e.g., preexistence of discontinuities and spatial variability, development of discontinuities), as well as monitor processes. The exploratory studies presented in this manuscript demonstrate the potential of x-ray imaging to provide an enhanced understanding of localization (e.g., during blade insertion and mass removal), the development of various open-mode discontinuities (e.g., desiccation cracks, roots, and ice lenses), and process-driven changes (e.g., cryogenic consolidation and chemo-osmosis). Several first-time observations for the processes explored in this manuscript include the formation of sharply defined low-density pipes upon mass removal, cryogenic suction consolidation during ground freezing, root growth transverse expansion and cell growth/invasion into sediment pores at the tip, and the split of desiccation cracks at the front.

The most persistent spatial and temporal trade-offs relate to the inherent link between range and resolution and the process-to-observation relative time scales.

X-ray absorption may not always be used to detect a cause (e.g., chemical diffusion or thermal fronts). However, it may still allow us to observe the effect of a process (e.g., chemo-osmotic consolidation or cryo-suction driven consolidation).

Exploratory studies documented in this manuscript show that insightful, high-impact findings can be made with relatively modest x-ray lab devices without having to resort to limited-access synchrotron sources.

ACKNOWLEDGMENTS

This research was conducted at Laboratoire 3SR, Grenoble. Funding was provided by Université Joseph Fourier, the U.S. National Science Foundation, and the Goizueta Foundation. The writers thank the two anonymous reviewers for their detailed and constructive remarks.

References

Alshibli, K. A., Cil, M. B., Kenesei, P., and Lienert, U., 2013, "Strain Tensor Determination of Compressed Individual Silica Sand Particles Using High-energy Synchrotron Diffraction," *Granular Matter*, Vol. 15, No. 5, pp. 517–530.

Alshibli, K. A. and Reed, A. H., Eds., 2010, *Applications of X-ray Microtomography to Geomaterials*, ISTE, London.

Andò, E., Hall, S. A., Viggiani, G., Desrues, J., and Bésuelle, P., 2012, "Grain-scale Experimental Investigation of Localised Deformation in Sand: A Discrete Particle Tracking Approach," *Acta Geotech.*, Vol. 7, No. 1, pp. 1–13.

Baruchel, J., 2000, *X-ray Tomography in Materials Science*, Editions Hermes, Paris.

Berg, S., Ott, H., Klapp, S. A., Schwing, A., Neiteler, R., Brussee, N., Makurat, A., Leu, L., Enzmann, F., Schwarz, J.-O., Kersten, M., Irvine, S., and Stampanoni, M., 2013, "Real-time 3D Imaging of Haines Jumps in Porous Media Flow," *Proc. Natl. Acad. Sci. U.S.A.*, Vol. 110, No. 10, pp. 3755–3759.

Besnard, G., Hild, F., and Roux, S., 2006, "'Finite-element' Displacement Fields Analysis from Digital Images: Application to Portevin–Le Châtelier Bands," *Exp. Mech.*, Vol. 46, No. 6, pp. 789–803.

Comina, C., Foti, S., Musso, G., and Romero, E., 2008, "EIT Oedometer: An Advanced Cell to Monitor Spatial and Time Variability in Soil with Electrical and Seismic Measurements," *Geotech. Test. J.*, Vol. 31, No. 5, pp. 564–572.

Dai, S., Santamarina, J. C., Waite, W. F., and Kneafsey, T. J., 2012, "Hydrate Morphology: Physical Properties of Sands with Patchy Hydrate Saturation," *J. Geophys. Res.*, Vol. 117, No. B11205.

Desrues, J., Chambon, R., Mokni, M., and Mazerolle, F., 1996, "Void Ratio Evolution inside Shear Bands in Triaxial Sand Specimens Studied by Computed Tomography," *Géotechnique*, Vol. 46, No. 3, pp. 529–546.

Desrues, J., Viggiani, G., and Bésuelle, P., Eds., 2006, *Advances in X-ray Tomography for Geomaterials*, ISTE, London.

Dysli, M., 1991, *Le Gel et Son Action sur les sols et les Fondations [Freezing and its effect on soils and foundations]*, Presses Polytechniques et Universitaires Romandes, Lausanne, France (in French).

Fusseis, F., Steeb, H., Xiao, X., Zhu, W.-L., Butler, I. B., Elphick, S., and Mäder, U., 2014, "A Low-cost X-ray-transparent Experimental Cell for Synchrotron-based Xray Microtomography Studies Under Geological Reservoir Conditions," *J. Synchrotron Rad.*, Vol. 21, pp. 251–253.

Gonzàles, C. and Sagaseta, C., 2001, "Patterns of Soil Deformations around Tunnels. Application to the Extension of Madrid Metro," *Comput. Geotech.*, Vol. 28, Nos. 6–7, pp. 445–468.

Gregory, P. J., Hutchison, D. J., Read, D. B., Jenneson, P. M., Gilboy, W. B., and Morton, E. J., 2003, "Non-invasive Imaging of Roots with High Resolution X-ray Microtomography," *Plant Soil*, Vol. 255, pp. 351–359.

Hainsworth, J. M. and Aylmore, L. A. G., 1983, "The Use of Computer Assisted Tomography to Determine Spatial Distribution of Soil Water Content," *Austr. J. Soil Res.*, Vol. 21, pp. 435–443.

Hall, S. A., 2013, "Characterization of Fluid Flow in a Shear Band in Porous Rock Using Neutron Radiography," *Geophys. Res. Lett.*, Vol. 40, No. 11, pp. 2613–2618.

Hall, S. A., Bornert, M., Desrues, J., Pannier, Y., Lenoir, N., Viggiani, G., and Bésuelle, P., 2010, "Discrete and Continuum Analysis of Localised Deformation in Sand Using X-ray Micro CT and Volumetric Digital Image Correlation," *Géotechnique*, Vol. 60, No. 5, pp. 315–322.

Hall, S. A., Wright, J., Pirling, T., Andò, E., Hughes, D. J., and Viggiani, G., 2011, "Can Inter-granular Force Transmission Be Identified in Sand? First Results of Spatially-resolved Neutron and X-ray Diffraction," *Granular Matter*, Vol. 13, No. 3, pp. 251–254.

Konrad, J.-M. and Duquennoi, C., 1993, "A Model for Water Transport and Ice Lensing in Freezing Soils," *Water Resour. Res.*, Vol. 29, No. 9, pp. 3109–3124.

Kulenkampff, J., Gründig, M., Richter, M., and Enzmann, F., 2008, "Evaluation of Positron-emission-tomography for Visualisation of Migration Processes in Geomaterials," *MIGRATION 2007, 11th International Conference on the Chemistry and Migration Behaviour of Actinides and Fission Products in the Geosphere, Physics and Chemistry of the Earth, Parts A/B/C*, Munich, Germany, pp. 937–942.

Materechera, S. A., Alston, A. M., Kirby, J. M., and Dexter, A. R., 1992, "Influence of Root Diameter on the Penetration of Seminal Roots Into a Compacted Subsoil," *Plant Soil*, Vol. 144, pp. 297–303.

Ng, C. W. W., Simons, E., and Menzies, B., 2004, *A Short Course in Soil-structure Engineering of Deep Foundations, Excavations and Tunnels*, Thomas Telford, London.

Otani, J. and Obara, Y., Eds., 2004, *X-ray CT for Geomaterials—Soils, Concrete, Rocks*, Balkema, Rotterdam, the Netherlands.

Peng, G. and Herrmann, H. J., 1994, "Density Waves of Granular Flow in a Pipe," *Phys. Rev. E*, Vol. 49, No. 3, p. R1796.

Pfeffer, W., 1893, "Druck und Arbeitsleistung durch wachsende Pflanzen," *Abhandlung der Königlich Sächsischen Gesellschaft der Wissenschaften*, Vol. 33, pp. 235–474.

Reiner, M., 1964, "The Deborah Number," *Phys. Today*, Vol. 17, No. 1, p. 62.

Roscoe, K. H., 1970, "The Influence of Strains in Soil Mechanics," *Géotechnique*, Vol. 20, No. 2, pp. 129–170.

Santamarina, J. C. and Jang, J., 2010, "Energy Geotechnology: Implications of Mixed Fluid Conditions," *5th International Conference on Unsaturated Soils*, Barcelona, Spain, Sept. 6–8, UPC (Universitat Politècnica de Catalunya), Barcelona, Spain.

Savioli, A., Viggiani, G., and Santamarina, J. C., 2014, "Root-Soil Mechanical Interaction," A. J. Puppala, P. Bandini, T. C. Sheahan, M. Abu-Farsakh, X. Yu, and L. R. Hoyos, Eds., *Geo-Congress 2014 Technical Papers*, *Geotechnical Special Publications (GSP) GSP 234–235*, ASCE, Reston, VA, pp. 3977–3984.

Sheng, D., Axelsson, K., and Knutsson, S., 1995, "Frost Heave Due to Ice Lens Formation in Freezing Soils 1. Theory and Verification," *Nordic Hydrol.*, Vol. 26, No. 2, pp. 125–146.

Sheppard, S., Sederman, A., Verganelakis, D., Johns, M., Mantle, M., and Gladden, L., 2003, "Probing Pore Scale Velocity Fields during Fluid Flow in Porous Media: Displacement Propagators of Non-Newtonian Fluids in Sedimentary Rocks," Technical Report, Schlumberger Cambridge Research, Department of Chemical Engineering, University of Cambridge, Cambridge, UK.

Shin, H. and Santamarina, J. C., 2011a, "Desiccation Cracks in Saturated Fine-grained Soils: Particle-level Phenomena and Effective-stress Analysis," *Géotechnique*, Vol. 61, No. 11, pp. 961–972.

Shin, H. and Santamarina, J. C., 2011b, "Open-mode Discontinuities in Soils," *Géotechnique Lett.*, Vol. 1, No. 4, pp. 95–99.

Smith, T. S., Bay, B., and Rashid, M., 2002, "Digital Volume Correlation Including Rotational Degrees of Freedom During Minimization," *Exp. Mech.*, Vol. 42, No. 3, pp. 272–278.

Stock, S. R., 2008, *Microcomputed Tomography: Methodology and Applications*, CRC Press, Boca Raton, FL.

Takano, D., Nagatani, H., Otani, J., and Mukunoki, T., 2004, "Evaluation of the Mechanism of Tunnel Face Failure Using X-ray CT Scanner," *Proceedings of the 9th International Symposium Numerical Models in Geomechanics*, Ottawa, Canada, Aug 25–27, 2004, pp. 415–420.

Terzaghi, K., 1936, "Stress Distribution in Dry and Saturated Sand above a Yielding Trap-door," *Proceedings of the International Conference of Soil Mechanics*, Cambridge, MA, June 26, 1936, Harvard University, Cambridge, Massachusetts, pp. 307–311.

Torrance, J. K., Elliot, T., Martin, R., and Heck, R. J., 2008, "X-ray Computed Tomography of Frozen Soil," *Cold Reg. Sci. Technol.*, Vol. 53, No. 1, pp. 75–82.

Viggiani, G. and Hall, S. A., 2012, "Full-field Measurements in Experimental Geomechanics: Historical Perspective, Current Trends and Recent Results," *Advanced Experimental Techniques in Geomechanics*, G. Viggiani, S. A. Hall, and E. Romero, Eds., ALERT-Geomaterials, Grenoble, France, pp. 3–67.

Viggiani, G., Lenoir, N., Bésuelle, P., Di Michiel, M., Marello, S., Desrues, J., and Kretzschmer, M., 2004, "X-ray Micro Tomography for Studying Localized Deformation in Fine-grained Geomaterials Under Triaxial Compression," *Comptes rendus Mécanique*, Vol. 332, pp. 819–826.